Journal of Neuroscience Methods 222 (2014) 97–105

Contents lists available at ScienceDirect

Journal of Neuroscience Methods

journal homepage: www.elsevier.com/locate/jneumeth

Computational Neuroscience

Automated interhemispheric surface extraction in T1-weighted MRI using intensity and symmetry information☆

Richard Nordenskjöld[a,*], Elna-Marie Larsson[a], Håkan Ahlström[a], Lars Johansson[a,b], Joel Kullberg[a]

[a] Department of Radiology, Uppsala University, Uppsala University Hospital, SE-751 85, Uppsala, Sweden
[b] AstraZeneca, Mölndal, Sweden

HIGHLIGHTS

- The whole head is divided with a max-flow/min-cut optimized surface.
- Both intensity and symmetry information is used for the surface optimization.
- No time consuming preprocessing steps are required.
- The interhemispheric surface is extracted in less than 30 s.

ARTICLE INFO

Article history:
Received 3 July 2013
Received in revised form 4 November 2013
Accepted 5 November 2013

Keywords:
Interhemispheric surface
Graph cut
Hemisphere separation
Midsagittal plane
Anterior commissure
Posterior commissure

ABSTRACT

Background: Localizing the human interhemispheric region is of interest in image analysis mainly because it can be used for hemisphere separation and as a preprocessing step for interhemispheric structure localization. Many existing methods focus on only one of these applications.
New method: Here a new *Intensity and Symmetry based Interhemispheric Surface extraction* method (ISIS) that enables both applications is presented. A combination of voxel intensity and local symmetry is used to optimize a surface from T1-weighted MRI.
Results: ISIS was evaluated in regard to cerebral hemisphere separation using manual segmentations. It was also evaluated in regard to being a preprocessing step for interhemispheric structure localization using manually placed landmarks.
Comparison with existing methods: Results were compared to cerebral hemisphere separations by BrainVisa and Freesurfer as well as to a midsagittal plane (MSP) extraction method. ISIS had less misclassified voxels than BrainVisa (ISIS: $0.119 \pm 0.114\%$, BrainVisa: $0.138 \pm 0.084\%$, $p = 0.020$). Freesurfer had less misclassified voxels than ISIS for one dataset (ISIS: $0.063 \pm 0.056\%$, Freesurfer: $0.049 \pm 0.044\%$, $p = 0.019$), but failed to produce usable results for another. Total voxel distance from all manual landmarks did not differ significantly between ISIS and the MSP method (ISIS: 4.00 ± 1.88, MSP: 4.47 ± 4.97).
Conclusions: ISIS was found successful in both cerebral hemisphere separation and as a preprocessing step for interhemispheric structure localization. It needs no time consuming preprocessing and extracts the interhemispheric surface in less than 30 s.

1. Introduction

The localization of the cerebral interhemispheric area is an important step in many different analyses of the brain. It is needed to separate the hemispheres for volumetric and morphological analysis. It also contains many important interhemispheric structures such as commissures and septum pellucidum (SP) that separates the lateral ventricles. The anterior (AC) and posterior (PC) commissures are landmarks often needed for spatial normalization (Talairach and Tournoux, 1988). The largest commissure, corpus callosum (CC), has been found associated with for example hypertension, cognition and Alzheimer's disease (Harris et al., 2008; Ryberg et al., 2007; Thomann et al., 2006). When segmenting the cerebral ventricular system the interhemispheric area separates the lateral ventricles and contains the third and fourth ventricles along with the cerebral aqueduct.

* Corresponding author at: MRT, Entrance 24, Uppsala University Hospital, SE-751 85 Uppsala, Sweden. Tel.: +46 186110167.
E-mail address: richard.nordenskjold@radiol.uu.se (R. Nordenskjöld).

0165-0270/$ – see front matter © 2013 The Authors. Published by Elsevier B.V. All rights reserved.
http://dx.doi.org/10.1016/j.jneumeth.2013.11.007

The interhemispheric area mostly contains cerebrospinal fluid (CSF), SP between the lateral ventricles, and the white matter (WM) commissures connecting the hemispheres. The term *area* is used since there is no surface defining the exact separation of the hemispheres, but rather an area covering the entire interhemispheric CSF, SP, and CC. There is, to the authors' knowledge, no clear definition where to separate CC. Since SP and interhemispheric CSF is included in the interhemispheric area, one could define the separation between these two using either a plane or a more complex shape.

A midsagittal plane (MSP) is a plane dividing the head into two globally or locally equal halves. MSP is often needed for spatial normalization, and the transformation into Talairach coordinate space (Talairach and Tournoux, 1988). Several automated methods for finding the MSP have been developed and some assume that the brain can be divided into two symmetrical hemispheres (Ardekani et al., 1997; Liu et al., 2001), while others look at local symmetry around a potential MSP (Hu and Nowinski, 2003; Prima et al., 2002; Stegmann et al., 2005; Volkau et al., 2006). A problem for all MSP methods is that the hemispheres are often not symmetric and that the interhemispheric area is curved (LeMay, 1976; Toga and Thompson, 2003). This makes a plane inaccurate for hemisphere separation in most cases. Several approaches for automated interhemispheric structure localization rely on the MSP as a preprocessing step (Ardekani and Bachman, 2009; Bhanuprakash et al., 2006; Nowinski et al., 2006; Verard et al., 1997).

Different methods providing a more accurate separation of the hemsipheres have been developed. Planes can be used to cut only the interhemispheric connections leaving the rest of the interhemispheric area to be located in a more advanced way (Dale et al., 1999; Kriegeskorte and Goebel, 2001). Some methods calculate shape bottlenecks in the brain tissue and separate the hemispheres at those locations (Mangin et al., 2004; Zhao et al., 2010). In Liang et al. (2007) a graph cut (GC, Boykov and Kolmogorov (2004)) based method is described, where seed points are placed based on tissue classification results, and the lateral ventricles have been "filled" before the separation. A common limitation for all these methods is that they rely on pre-segmentation of brain tissue and/or structure localization.

MSP has been seen as an accurate preprocessing step for structure localization, but fails for hemisphere separation. Hemisphere separation is often performed following structure or tissue segmentation. By removing the need for pre-segmentation and other preprocessing steps, the execution time can be heavily reduced. If features from both approaches were to be combined, a single method for both hemisphere separation and structure localization could be created.

In this paper we present and evaluate *Intensity and Symmetry based Interhemispheric Surface extraction* (ISIS). A method that combines intensity and symmetry information to extract an interhemispheric surface from T1-weighted MRI, without any time consuming preprocessing, that can be used for both cerebral hemisphere separation and as a preprocessing step for interhemispheric structure localization.

2. Materials and methods

ISIS uses a novel cost function to optimize the hemispherical separation of an entire T1-weighted image using GC (Boykov and Kolmogorov, 2004). GC is a graph based max-flow/min-cut algorithm that labels an image into two classes by representing it as a graph with costs assigned to each edge. Each voxel is represented by a node in a graph which is connected to other nodes by edges. There are two different types of edges in the graph. One type for connecting nodes to each other (n-cost), and another for connecting nodes to different labels (t-cost). The cost that an edge has defines how well connected the two adjacent nodes are. A low cost favors the method to "cut" that edge. The optimal cut is defined by the edges generating the lowest sum of edge costs while separating the graph into two unconnected subgraphs.

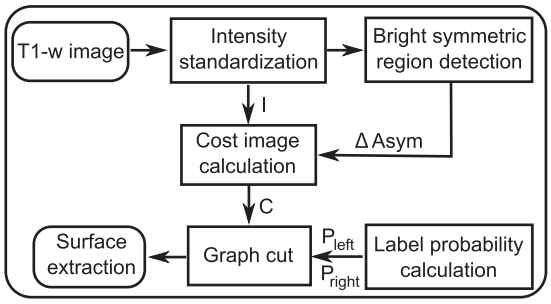

Fig. 1. Flowchart for ISIS.

An overview of the ISIS is given in Fig. 1. Intensity (I) is used in combination with local symmetry (ΔAsym) to create a cost image (C). A GC method using C as n-costs and probability of belonging to a certain hemisphere (P) as t-cost is then used to find the optimized interhemispheric surface. The surface is calculated to span the entire image, and does not require any skull-stripping or other time consuming preprocessing before being calculated.

For a more detailed explanation and justification of the parameters used in this section, see Appendix A.

2.1. Image orientation

The method described assumes that the input images are sagitally oriented and z denotes the coordinate in the sagittal direction. It is also assumed that the images are roughly oriented having only small yaw and roll angles of the head with respect to the MR scanner coordinates and that the head is roughly centered in the sagittal direction.

2.2. Intensity standardization

Since T1-weighted MRI has arbitrary units, the image intensities were scaled between 0 and 1. Before scaling, intensity outliers were removed in order to decrease the effect of noise. All voxels having an intensity outside the range of 1–99% in the intensity histogram were set to the closest intensity included in the range. For further reference, this standardized image is referred to as I. If this image alone defined the n-costs in the GC optimization, the resulting cut would be drawn to CSF and other dark regions. Since bright structures such as CC and SP needs to be cut, additional information needs to be used before calculating the final n-costs.

2.3. Bright symmetric region detection

The interhemispheric area consists of bright non-CSF regions such as CC and SP. In order to favor these regions in the GC optimization, they need to have a lower n-cost than the surrounding CSF. All bright structures located in the interhemispheric area have a high local symmetry in the lateral–medial direction. An assumption that the interhemispheric region is more symmetrical than other regions in the brain motivates the use of local symmetric maxima (ΔAsym) to favor interhemispheric surface placement. Since higher symmetry should give a lower n-cost, it is calculated indirectly as an asymmetry measure. The lowest n-cost is desired in the middle of the structure, and therefore the region for symmetry calculation needs to be large enough to include the entire structure. ΔAsym was calculated in the lateral–medial direction on axial slices. The

calculation of ΔAsym was performed in two steps. Firstly a local symmetry measure (Asym) was determined, and secondly Asym was used to calculate ΔAsym. The symmetry was calculated as in Eq. (1)

$$Asym(z) = \frac{\sum_{i=1}^{W_{vx}/2} |I(z-i) - I(z+i)| e^{-(i-1)^2/2(W_{vx}/2)^2}}{I(z)\sum_{i=1}^{W_{vx}/2} e^{-(i-1)^2/2(W_{vx}/2)^2}} \quad (1)$$

where z is the lateral–medial coordinate of a voxel being measured, and i is the voxel offset. Since the purpose of the symmetry was to lower the n-costs in bright areas, the symmetry was weighted by $I(z)$. A window (W_{vx}) of 48 mm, rounded to the nearest voxel, was empirically determined. This to ensure complete coverage of the brain stem and other structures, while not reaching outside of the brain. To reduce the risk of including unwanted voxels in the edges of the window, a distance based weight was used as seen in Eq. (1).

Once all voxels had been assigned a symmetry value, local properties of the symmetry variations were calculated as in Algorithm 2.1 using a window size of 6 mm converted to voxels in the same way as described above (ΔW_{vx}).

Algorithm 2.1. ΔAsym calculation

$\{i \in \mathbb{N} : \leq i \leq \Delta W_{vx}\}$
$left \leftarrow mean(Asym(z+i))$
$right \leftarrow mean(Asym(z-i))$
if $left > Asym(z)$ AND $right > Asym(z)$ **then**
  $\Delta Asym(z) \leftarrow Asym(z)/min(left, right)$
else
  $\Delta Asym(z) \leftarrow 1.0$
end if

The smallest of the two means was used to lessen sudden changes on only one side of the voxel at location z, making the method a little more robust against pathologies. The resulting ΔAsym image promotes the locally most symmetrical areas by assigning them a value less than 1.0, while other areas remain neutral with a value of 1.0.

2.4. Cost image calculation

The final cost image to be used in the GC optimization was created by combining I and ΔAsym according to Eq. (2).

$$C = (I * \Delta Asym^a)^b \quad (2)$$

The balance between intensity and symmetry can be adjusted with a and the contrast between dark and bright areas with b. This image was used to initiate all n-costs in the GC optimization.

2.5. Label probability calculation

Given an image that is aligned along for example the hypophysis-fastigium (HYFA) or AC-PC line, the probability of a voxel belonging to a specific side of the head can be based on the lateral distance from the image center. Since the head may be somewhat misaligned and the interhemispheric area may deviate from the heads center, the probabilities were set to small values in this area. The farther from the heads center, the more certain one can be of the side to which the voxels belongs. The probabilities were calculated as in Eq. (3)

$$P(z) = e^{-\frac{(z-\mu)^2}{2\sigma^2}} \quad (3)$$

where μ is 0 for the left side(P_{left}), and z_{max} for the right side (P_{right}) of the head. σ is $z_{max}/3$ for both P (Fig. 2).

Table 1
Description of the datasets used for method evaluation.

Dataset	n	Subjects	Age
1	13	General population	75
2	15	General population	80
3	9	NPH[a]	Mix

[a] Normal pressure hydrocephalus.

2.6. Graph cut setup

In ISIS, the labels represented the different hemispheres and the graph had 6-adjacency. The t-costs were set according to P (Eq. (3)) and the n-cost from i to j according to $0.5C(i) + C(j)$). Examples of the costs used for GC are illustrated in Fig 2.

2.7. Surface extraction

The final step of the method is to extract the surface from the GC labeling results. Since GC does not cut voxels but the edges between them, the surface was extracted as the set of mean coordinates of each voxel pair connected by a cut edge.

2.8. Evaluation

2.8.1. Environment

The method was implemented in C++ and all evaluations were performed using a laptop with a 2.0 GHz dual core processor and 4 GB RAM under the Windows 7 x64 operating system. In all performed evaluations, a and b in Eq. (2) were both set to 2.0.

2.8.2. Datasets

Four different datasets were used in the evaluation. Specific imaging parameters for datasets 1–3 are given below with subject information given in Table 1. All subjects in these datasets were scanned with clinical MRI scanners (Achieva, Philips Healthcare, Best, The Netherlands). This study was approved by the local ethics committee.

Dataset 1 and 2 were both scanned with a 3D gradient echo sequence at 1.5 Tesla (flip angle: 8°, echo time: 4 ms, repetition time: 8.6 ms, in-plane resolution: 0.94^2 mm, slice thickness: 1.2 mm). Dataset 3 was scanned with a 3D gradient echo sequence at 3 Tesla (flip angle: 8°, echo time: 3.79 ms, repetition time: 8.27 ms, 1 mm isotropic voxels).

These datasets were used having their original orientation without being subjected to any alignment.

The fourth dataset contained 18 simulated T1-w MRI of a normal brain from the BrainWeb database (Cocosco et al., 1997; Collins et al., 1998). This dataset consists of a single brain having different combinations of noise ([0, 1, 3, 5, 7, 9] %) and intensity non-uniformity ([0, 20, 40] %).

2.8.3. Hemisphere separation

ISIS was compared in terms of cerebral hemisphere separation to the semi-automated hemisphere separation in BrainVisa version 4.1.1 (Mangin et al., 2004), and to the automated hemisphere separation in Freesurfer version 5.1.0 (Dale et al., 1999).

BrainVisa requires the user to specify points in AC, PC, interhemispheric fissure, and the left hemisphere. The hemispheres are then divided without further interaction using morphological operations to locate shape bottlenecks connecting the hemispheres. The resulting image (*voronoi*) contains gray matter (GM) and WM with each voxel labeled according to the hemisphere it is located in.

Freesurfer is a fully automated method that divides the hemispheres using the plane producing the minimal cutting area through WM. The hemispheres are then expanded to include GM.

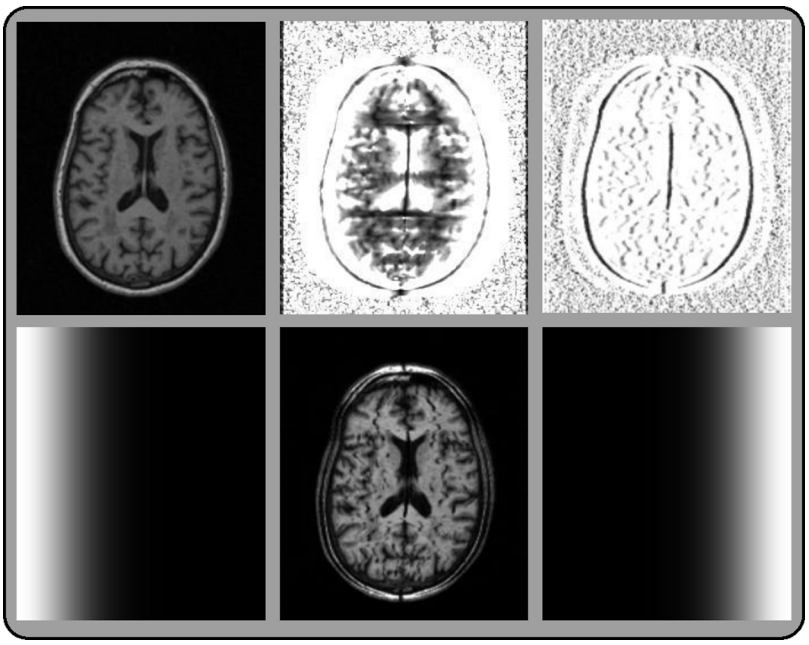

Fig. 2. Cost image preparation examples. The darker the intensity the lower the cost. Top row from left to right: intensity image (I), Asym image, ΔAsym image. Bottom row from left to right: label probability for left side (P_{left}), final cost image (C), label probability for right side (P_{right}).

The resulting image (*ribbon*) contains GM and WM with each voxel labeled according to tissue type and hemisphere. For dataset 3, containing normal pressure hydrocephalus (NPH) subjects, Freesurfer failed to produce accurate results. This is most likely due to the large difference in appearance between the NPH subjects and the prior knowledge used in Freesurfer. Rather than manually correcting the steps in Freesurfer, this method was excluded from evaluations involving this dataset.

The hemisphere labeling in both BrainVisa and Freesurfer excludes CSF while ISIS labels all voxels in the image. Therefore, only voxels labeled by all compared methods were taken into consideration in the evaluation. Reference segmentations were performed manually by two operators. The manual segmentation was performed on every tenth axial slice in the brain mask generated by BrainVisa (with visible aid of the original T1-w image). The segmented slices were the ones that contained any brain and had an axial slice number evenly dividable by ten. The location of the manual segmentations thus varied between subjects. Separate comparisons with the references created by each operator were made and the mean error was used in the evaluation. A paired t-test was used to determine if the errors differed between the methods.

2.8.4. Landmark localization

ISIS was also compared to an in-house implementation of the MSP extraction described in Hu and Nowinski (2003) to investigate if the extracted surface can be used as a preprocessing step for interhemispheric structure localization. Manually selected landmarks were placed on six different locations (Fig. 3) in all datasets by one operator. The shortest distance in the lateral–medial direction between each landmark and the extracted surface was calculated and used as a measure of error. The landmarks were placed with subvoxel accuracy. In the evaluation, all landmarks placed in SP were measured together as they represent the same structure.

A Wilcoxon signed-rank test was used to determine if the errors differed between the methods.

2.8.5. Additional preprocessing

Additional evaluations of ISIS were conducted to see the effects of skullstripping and intensity non-uniformity correction. The skullstripped (*brain.mgz*) and intensity non-uniformity corrected (*T1.mgz*) images, both output from Freesurfer, were used. After a conversion from the coordinate system used in Freesurfer back to native space, brain.mgz was used as a mask to skullstrip the original images in the datasets. The reason for not using brain.mgz directly was because it does not contain the original intensity values of the input image. T1.mgz could be used directly after the conversion to native space. Since Freesurfer failed in processing dataset 3, this evaluation was performed using datasets 1 and 2. Both hemisphere separation and landmark localization were evaluated using the same references, landmark placements, and statistical tests as described above.

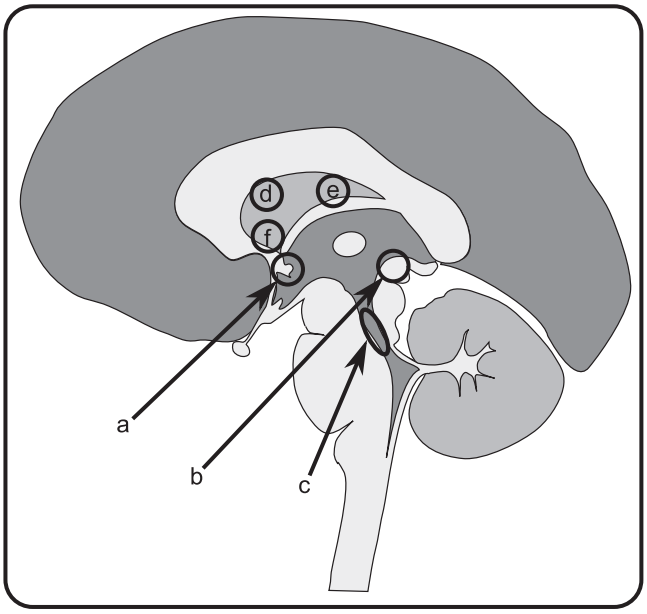

Fig. 3. Interhemispheric structures used for evaluation. Points were manually placed in the areas indicated with circles or ellipses. (a) Anterior commissure. (b) Posterior commissure. (c) Cerebral aqueduct. (d–f) Different locations on septum pellucidum.

Table 2
Results of hemisphere separation, given in percentage of misclassified voxels (mean ± SD), when compared to a manual reference. BrainVisa and Freesurfer are both compared to ISIS.

Dataset	ISIS	BrainVisa (p)	Freesurfer (p)	*n*
1–3	0.119 ± 0.114	0.138 ± 0.084 (**0.020**)	-	37
1	0.061 ± 0.039	0.105 ± 0.041 (**0.003**)	0.059 ± 0.026 (*NS*[a])	13
2	0.063 ± 0.056	0.094 ± 0.047 (**0.003**)	0.049 ± 0.044 (**0.019**)	15
3	0.295 ± 0.063	0.261 ± 0.054 (*NS*[a])	-	9

Bold indicates significant values ($p < 0.05$).
[a] Not significant ($p > 0.05$.)

2.8.6. Noise and intensity non-uniformity

To evaluate how robust ISIS is against noise and intensity non-uniformity, simulated MRI from the BrainWeb database was used. For each combination of noise and intensity non-uniformity, both hemisphere separation and landmark localization was evaluated. The reference in these evaluations was the automated anatomical labeling template (Tzourio-Mazoyer et al., 2002). This template consists of manually delineated regions in the same brain as in the BrainWeb images. Most of WM is excluded while the cortical labeling expands into CSF in the template. The *anatomical model of normal brain* from which the dataset was simulated (also provided by BrainWeb) was used to remove CSF from the template resulting in the reference used. Both hemisphere separation and landmark localization were evaluated.

3. Results

The cost image creation darkens the locally most symmetrical areas. An example of this is illustrated in Fig. 4, where the final cost image (Fig. 4d) shows a dark path through CC as well as a darkened SP.

Typical results from ISIS, BrainVisa, and Freesurfer are shown in Fig. 5. When results from ISIS and BrainVisa were compared to a manually created reference, ISIS had fewer misclassified voxels than BrainVisa when considering all datasets. ISIS proved to be more accurate for datasets 1 and 2 but not for dataset 3 (Table 2). Freesurfer had less misclassified voxels than ISIS for dataset 2, but failed to produce usable results for dataset 3.

While Freesurfer has less misclassified voxels for dataset 2, the method failed for dataset 3. Shown in Fig. 6 is one of the worst results. The Freesurfer results for this dataset had in common that brain tissue was unlabeled or excluded.

Interhemispheric structure evaluation showed no significant differences between compared methods (Table 3) when considering all datasets. This was also true when considering each dataset individually.

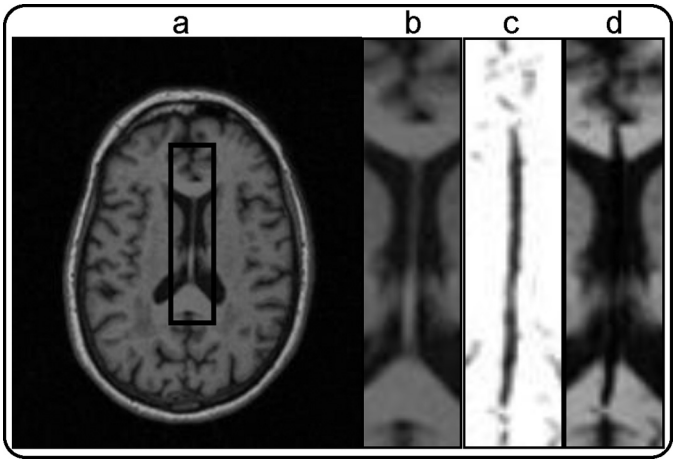

Fig. 4. Example of cost image creation. (a) Original input image with marked area to be magnified. (b) Magnified area showing original input image. (c) Symmetry image (ΔAsym). (d) Final cost image used for graph cut optimization.

Table 3
Absolute voxel distance (mean± SD) between interhemispheric surface/plane and landmarks in all datasets.

Landmark	ISIS	MSP (p)	*n*
Anterior commissure	0.47 ± 0.34	0.73 ± 0.94 (*NS*[a])	37
Posterior commissure	0.58 ± 0.37	0.74 ± 0.86 (*NS*[a])	37
Cerebral aqueduct	0.52 ± 0.32	0.79 ± 1.05 (*NS*[a])	37
Septum pellucidum	0.81 ± 0.59	0.74 ± 0.80 (*NS*[a])	111[b]
Total error	4.00 ± 1.88	4.47 ± 4.97 (*NS*[a])	222

[a] Not significant ($p > 0.05$).
[b] Three landmarks placed in the structure.

Resulting errors for each individual landmark are shown in Fig. 7. ISIS had an average error of less than 1 voxel for each landmark.

Presented in Table 4 are the errors produced by ISIS when skull-stripping and intensity non-uniformity correction had been applied to datasets 1 and 2. Corresponding evaluations for landmark localization is presented in Table 5. ISIS had less misclassified voxels without additional preprocessing and the only benefit when ISIS is used for landmark localization is skullstripping when septum pellucidum is to be located.

Results for ISIS when images with different noise and intensity non-uniformity were processed are shown in Fig. 8. As the noise is increased the number of misclassified voxels decreases. An example of a region benefiting from additional noise is highlighted in Fig. 8(c) and (d). Only minor changes in the landmark evaluation were seen when varying noise and intensity non-uniformity.

4. Discussion

A new method for interhemispheric surface extraction has been presented and evaluated. ISIS was compared to other existing methods and proved to have comparable accuracy regarding both cerebral hemisphere separation as well as when used as a preprocessing step for structure localization. No time consuming preprocessing steps are used and the surface is extracted in less than 30 s.

When separating the hemispheres, BrainVisa tends to remove SP from the tissues taken into consideration. SP is connected to both fornix and CC. The connections between these structures thusly defines where they should be separated. BrainVisa has difficulties in these structures (Fig. 5b). ISIS has difficulties in

Table 4
Hemisphere separation error when images in dataset 1 and 2 were skullstripped or intensity non-uniformity corrected (INU corrected). The error is given in percentage of misclassified voxels (mean ± SD) when compared to a manual reference. *P*-values are calculated when compared to results from non-preprocessed datasets.

Dataset	Skullstripped (p)	INU corrected (p)	*n*
1+2	0.068 ± 0.051 (**0.002**)	0.072 ± 0.053 (**0.000**)	28
1	0.070 ± 0.048 (**0.000**)	0.076 ± 0.048 (**0.002**)	13
2	0.067 ± 0.056 (*NS*[a])	0.070 ± 0.059 (**0.006**)	15

Bold indicates significant values ($p < 0.05$).
[a] Not significant ($p > 0.05$).

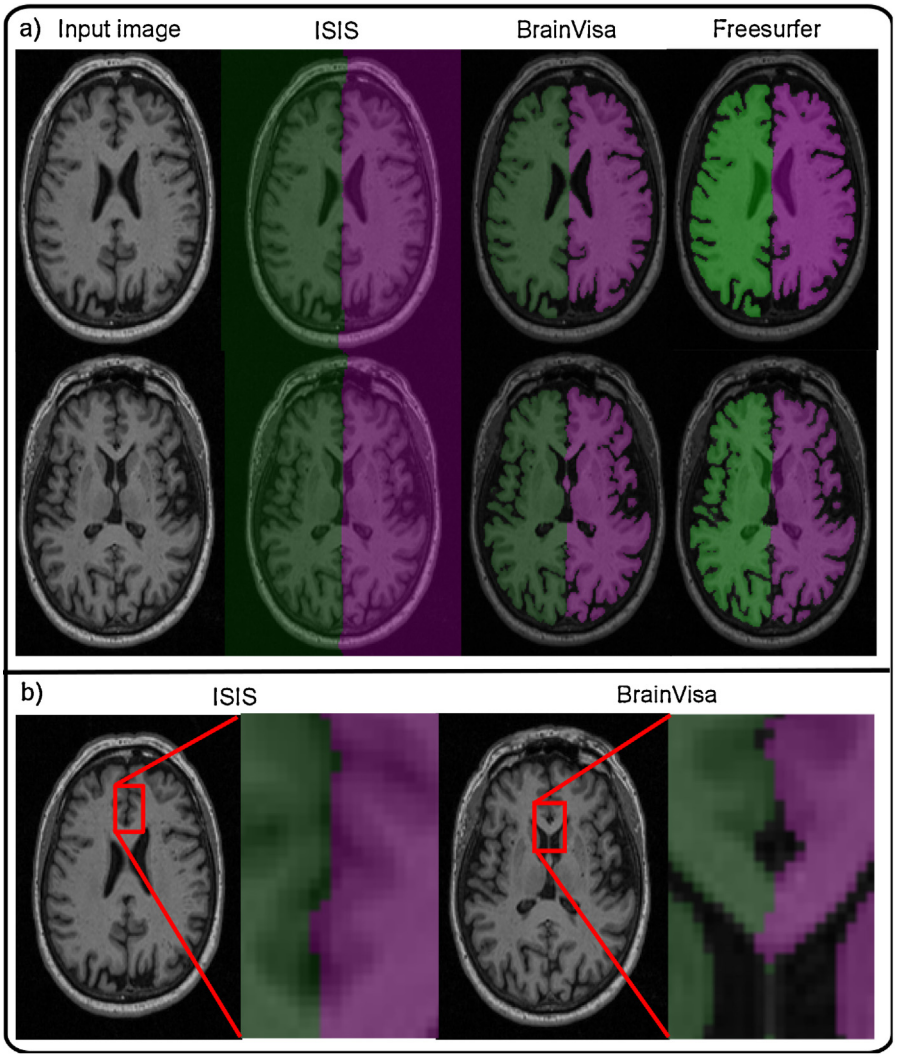

Fig. 5. Typical separation results. (a) Two examples of results from ISIS, BrainVisa and Freesurfer. As can be seen BrainVisa only labels white and gray matter while Freesurfer in addition to this also labels the lateral ventricles. ISIS labels the entire image. (b) Typical sources of miss-classification for ISIS and BrainVisa. ISIS tends to "cut corners" in high curvature areas and BrainVisa has problem separating corpus callosum. Freesurfer did not show signs of producing any typical errors.

high curvature parts of the interhemispheric area. This is due to the use of GC. A minimal cut does not necessarily mean that it will include the lowest cost edges. A straight cut has to include fewer edges than a curved one. If the sum of a few connected high cost edges is less than the sum of the connected low cost edges in a desired cut, GC will "cut corners". Freesurfer showed no clear signs of having difficulties in any specific structure or area.

Dataset 3 contained subjects with high-grade ventricular enlargement. SP was less visible, the ventricles were commonly not evenly enlarged, and the symmetrical properties in this region were reduced in these images. ISIS therefore had some difficulties with the separation of CC, which explains the increased misclassification of voxels in this dataset. BrainVisa was less affected as it does not depend on the ventricular symmetry or SP. Freesurfer did not produce usable results for this dataset, most likely because it is an atlas based method that transforms the image into Talairach space before intensity normalization and skullstripping is performed. As can be seen in Fig. 6 parts of the brain has been removed, indicating that it is the skullstripping that has failed. This could have in turn been caused by an incorrect preceding Talairach transformation.

Table 5
Absolute mean distance in voxels (mean ± SD) between the surface extracted by ISIS and all landmarks in dataset 1 and 2. Skullstripped and intensity non-uniformity corrected (INU corrected) versions of datasets 1 and 2 were compared to results when using the original non-preprocessed datasets.

Landmark	Original	Skullstripped (p)	INU corrected (p)	*n*
Anterior commissure	0.43 ± 0.34	0.49 ± 0.40 (*NS*[a])	0.40 ± 0.29 (*NS*[a])	28
Posterior commissure	0.48 ± 0.28	0.48 ± 0.28 (*NS*[a])	0.48 ± 0.28 (*NS*[a])	28
Cerebral aqueduct	0.52 ± 0.30	0.52 ± 0.30 (*NS*[a])	0.52 ± 0.31 (*NS*[a])	28
Septum pellucidum	0.65 ± 0.48	0.59 ± 0.44 (**0.043**)	0.63 ± 0.43 (*NS*[a])	84
Total error	3.37 ± 1.33	3.27 ± 1.24 (*NS*[a])	3.29 ± 1.29 (*NS*[a])	168

Bold indicates significant values ($p < 0.05$).
[a] Not significant ($p > 0.05$).
[b] Three landmarks placed in the structure.

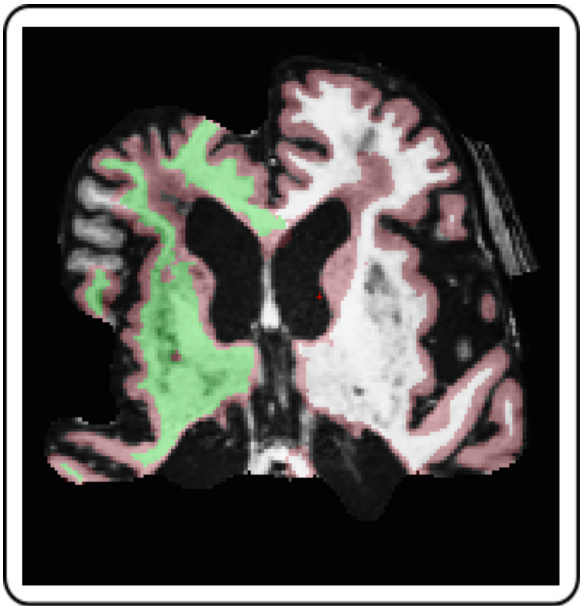

Fig. 6. Freesurfer results from uncorrected normal pressure hydrocephalus subject. One of the worst cases for Freesurfers hemisphere division. The axial slice shows parts of the brain excluded and unlabeled brain tissue voxels.

The similar results between methods in the interhemispheric structure evaluation could be because both compared methods rely on symmetrical features in the regions where landmarks were placed. Another factor was that no subjects in the datasets were seen to have a severely curved interhemispheric area. If this was the case it would be likely that the MSP method would decrease in accuracy more than ISIS. A disadvantage with ISIS is that it relies on symmetrical features. This makes the method unreliable in subjects with pathologies in or close to the white matter structures that are assumed to be symmetrical. This is however also a disadvantage in symmetry-based MSP methods.

As ISIS does not extract a surface with subvoxel accuracy, a small error is to be expected when compared to landmarks placed with subvoxel accuracy in the center of each evaluated structure. Despite a reported error, a structure may still be visible in the extracted surface/plane since it is represented by a single point having no thickness.

ISIS showed little signs of benefiting from additional preprocessing. Both skullstripping and intensity non-uniformity correction increased or produced a similar amount of misclassified voxels. For the use of ISIS as a preprocessing step for interhemispheric structure localization, the only benefit was to perform skullstripping when locating septum pellucidum. These results can likely be improved by changing the balance between symmetry and intensity in Eq. (2), but was not investigated in this study. As the parameters a and b were optimized on images that had undergone none of the tested preprocessing steps (A.4), these types of images are likely to be divided more accurately than the preprocessed ones.

The decrease in estimation error of ISIS when increasing the noise in an image is most likely due to the balance between parameters a and b. When there is no or low noise in an image, it is possible to find very good local symmetries. A near perfect symmetry can overpower the intensity part of the cost calculation in Eq. (2), making it less expensive to place a cut in symmetric areas lying next to the interhemispheric fissure than in it. By visual inspection it was determined that this is the case in this evaluation. In Fig 5 it can be seen how the cut more accurately follows the interhemispheric fissure as the noise is increased. The results in Fig. 8 b) are divided in three levels of error. These are exactly 1/6 voxel apart. The effect on the error when the extracted surface passes 1 voxel further away from a landmark while all others are passed in the same way will be exactly 1/6. This indicates how small the differences are when adjusting the noise and intensity non-uniformity in an image.

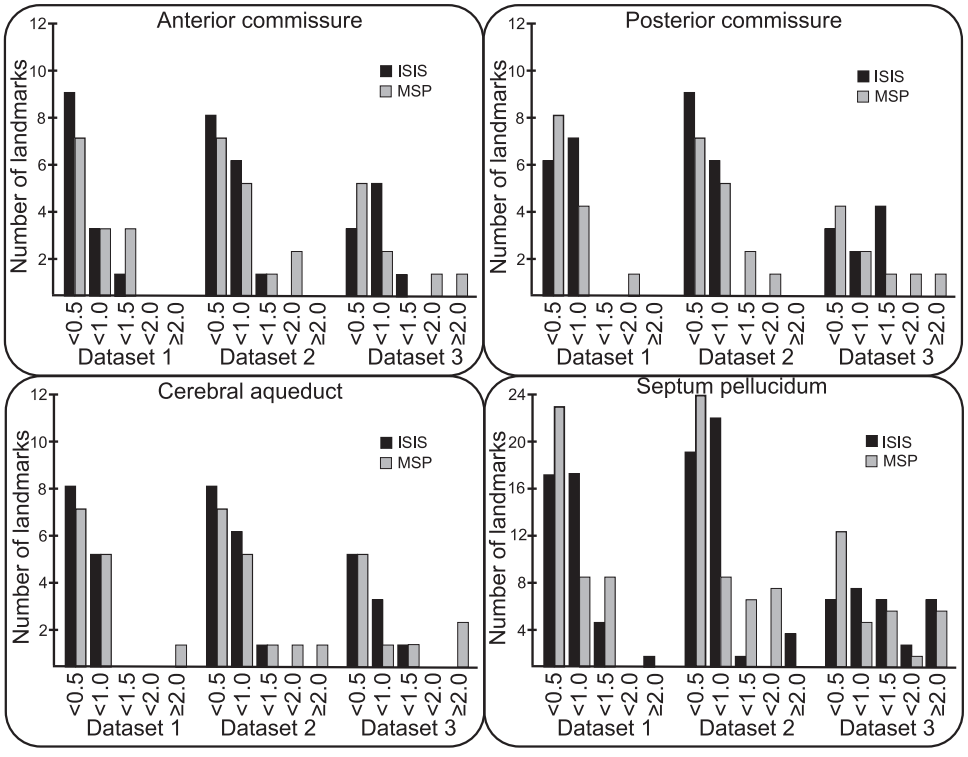

Fig. 7. Distribution of structure localization errors for each respective landmark. All errors are in voxels. Each subject had one point in each structure, except septum pellucidum which contained three points. For details about the datasets see Table 1.

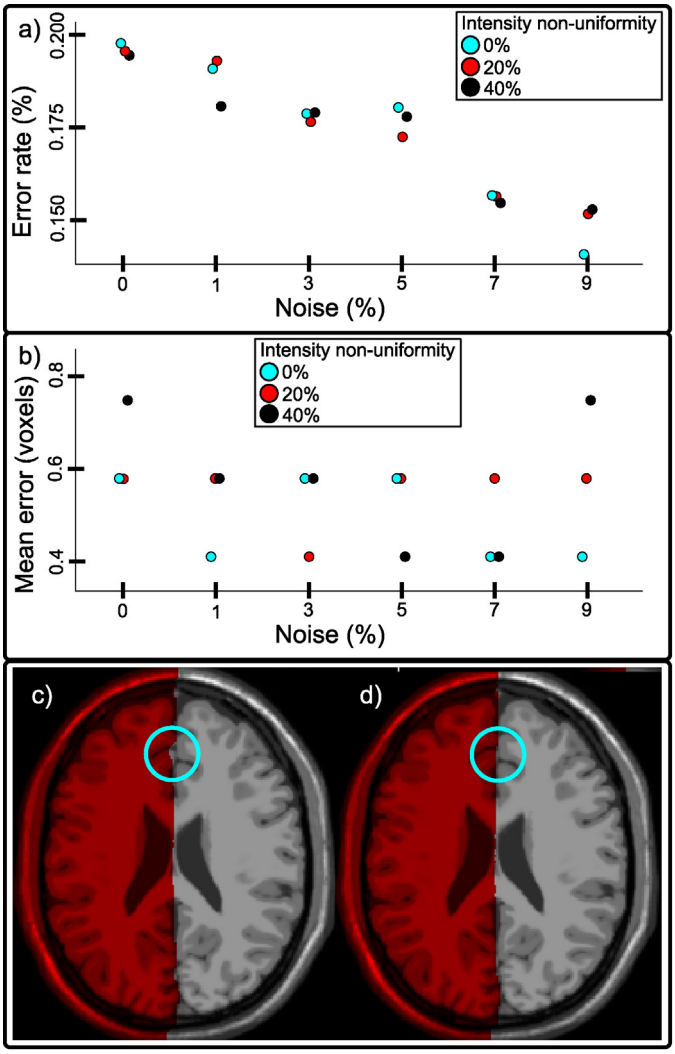

Fig. 8. Noise and intensity non-uniformity results for ISIS. (a) Hemisphere separation error. (b) Absolute mean distance between the extracted interhemispheric surface and all landmarks. (c) and (d) are results of hemisphere separation for 0% and 9% noise respectively, both overlayed on the image containing 0% noise. A clear difference is highlighted in both images.

Although ISIS extracts a surface dividing the entire head into two halves, no evaluation of cerebellar hemisphere division was performed as this goes beyond the scope of this paper.

In theory it should be possible to run the algorithm on images other than T1-weighted MRI. As long as the interhemispheric area visually consists of symmetrical structures and distinguishable CSF, small adjustments of a and b or inverting the intensities in I might suffice.

A limitation in ISIS is that it assumes the input images to have a specific orientation. If this assumption does not hold for an input image, it first needs to be roughly aligned before ISIS can be used.

The presented results suggest that ISIS can be used to separate the cerebral hemispheres and as a preprocessing step for interhemispheric structure localization. As the whole image is separated in two, the fourth ventricle and cerebral aqueduct can also be analyzed.

4.1. Conclusions

In this paper we have presented and evaluated ISIS. A new method for interhemispheric surface extraction from T1-weighted MRI. It extracted the surface in less than 30 s without relying on any time consuming preprocessing steps, produced robust results that are comparable to that of existing methods. It proved to be well suited for both cerebral hemisphere separation and as a preprocessing step for interhemispheric structure localization.

Appendix A. Parameter justification

A.1. Local symmetry window size W_{vx}

The size of the symmetry window was determined based on the size of interhemispheric structures of interest. If the window size used in the local symmetry calculation (Eq. (1)) was smaller than a homogeneous structure of interest, the structure would not necessarily have a dark path through it's center. The larger the window, the more sensitive the measure becomes to brain asymmetries and pathologies. To decrease the risk of these effects while still collecting symmetry information, weights decreasing with the distance from the center voxel were used.

A.2. Distance from center weight term

Higher contrast between septum pellucidum and surrounding CSF makes the interhemispheric surface follow the septum pellucidum better. If the contrast is low, the symmetry measure will favor the middle of the lateral ventricles, increasing the cost advantage of this CSF when combined with the intensity image. This becomes more apparent if the lateral ventricles are asymmetrical, otherwise the septum pellucidum and the center of the ventricles are located in nearly the same place. This effect is reduced by the "distance from center" weight term in Eq. (1).

A.3. Regional symmetrical maxima window size ΔW_{vx}

The local window size used in the ΔAsym calculation (Algorithm 2.1) was set to be large enough to cover at least a few voxels to lessen the effect of noise. The window size also had to be small to prevent multiple symmetrical areas from being contained in the same window. If this would occur, the resulting ΔAsym would be unreliable as it would add symmetrical area denseness to the desired local relative symmetry.

A.4. Cost function parameters a and b

The balance variables a and b in Eq. (2) were determined through a series of tests on a dataset (n=9) not included in the evaluation. The value of a is mostly dependent on the contrast between septum pellucidum and surrounding CSF. The symmetry factor has to suppress the intensity of septum pellucidum to a lower level than CSF to favor a cut in this area. If a is too high, other symmetrical areas that lie outside the desired path have too much influence on the resulting path. GC locates the cut that has the lowest sum of costs independent of the number of edges included in the cut. This increases the importance of a balanced contrast adjusted with b. The resulting cost image needs to show contrast between the desired and undesired paths. If there is too little contrast, GC tends to create a cut that is too smooth, as it can be cheaper to cut a few middle cost edges than many low cost ones. If the contrast is too high the chance of the cut taking undesired detours increase, which becomes the case when the desired cutting path contains some edges with high cost. Tests gave the most accurate results when a was 1.5–2.5 and b was 1.0–2.5 (SD of error was 6.11%). These tests showed that the cost image creation is robust when choosing these parameters as there is a span in numbers giving good results.

A.5. Label probabilities P_{left} and P_{right}

The label probabilities are starting estimates and should not have much influence close to the interhemispheric region. There, it should be the n-costs connecting image voxels that is the determining factor for the separation. Therefore a standard deviation of 1/3 of the image width was used in the Gaussian distribution (Eq. (3)). The middle of the image then has a probability of around 1/3 of belonging to either label. As the n-costs are between 0 and 1, this is a good level for the t-costs to be the submissive factor in low n-cost areas.

References

Ardekani BA, Bachman AH. Model-based automatic detection of the anterior and posterior commissures on MRI scans. NeuroImage 2009];46:677–82.

Ardekani BA, Kershaw J, Braun M, Kanno I. Automatic detection of the mid-sagittal plane in 3-D brain images. IEEE Trans Med Imaging 1997];16:947–52.

Bhanuprakash K, Hu Q, Aziz A, Nowinski W. Rapid and automatic localization of the anterior and posterior commissure point landmarks in MR volumetric neuroimages. Acad Radiol 2006];13:36–54.

Boykov Y, Kolmogorov V. An experimental comparison of min-cut/max-flow algorithms for energy minimization in vision. IEEE Trans Pattern Anal Mach Intell 2004];26:1124–37.

Cocosco CA, Kollokian V, Kwan RKS, pike GB, Evans AC. Brainweb: online interface to a 3D MRI simulated brain database. In: NeuroImage; 1997].

Collins DL, Zijdenbos AP, Kollokian V, Sled JG, Kabani NJ, Holmes CJ, et al. Design and construction of a realistic digital brain phantom. IEEE Trans Med Imaging 1998];17:463–8.

Dale AM, Fischl B, Sereno MI. Cortical surface-based analysis. i. segmentation and surface reconstruction. NeuroImage 1999];9:179–94.

Harris P, Alcantara DA, Amenta N, Lopez OL, Eiriksdottir G, Sigurdsson S, et al. Localized measures of callosal atrophy are associated with late-life hypertension: Ages-reykjavik study. NeuroImage 2008];43:489–96.

Hu Q, Nowinski WL. A rapid algorithm for robust and automatic extraction of the midsagittal plane of the human cerebrum from neuroimages based on local symmetry and outlier removal. NeuroImage 2003];20:2153–65.

Kriegeskorte N, Goebel R. An efficient algorithm for topologically correct segmentation of the cortical sheet in anatomical mr volumes. NeuroImage 2001];14:329–46.

LeMay M. Morphological cerebral asymmetries of modern man, fossil man, and nonhuman primate. Ann N Y Acad Sci 1976];280:349–66.

Liang L, Rehm K, Woods RP, Rottenberg DA. Automatic segmentation of left and right cerebral hemispheres from MRI brain volumes using the graph cuts algorithm. NeuroImage 2007];34:1160–70.

Liu Y, Collins RT, Rothfus WE. Robust midsagittal plane extraction from normal and pathological 3-d neuroradiology images. IEEE Trans Med Imaging 2001];20:175–92.

Mangin JF, Riviere D, Cachia A, Duchesnay E, Cointepas Y, Papadopoulos-Orfanos D, et al. A framework to study the cortical folding patterns. Neuroimage 2004];23:S129–38.

Nowinski WL, Qian G, Bhanu Prakash KN, Hu Q, Aziz A. Fast talairach transformation for magnetic resonance neuroimages. J Comput Assist Tomogr 2006];30:629–41.

Prima S, Ourselin S, Ayache N. Computation of the mid-sagittal plane in 3-d brain images. IEEE Trans Med Imaging 2002];21:122–38.

Ryberg C, Rostrup E, Stegmann MB, Barkhof F, Scheltens P, van Straaten EC, et al. Clinical significance of corpus callosum atrophy in a mixed elderly population. Neurobiol Aging 2007];28:955–63.

Stegmann MB, Skoglund K, Ryberg C. Mid-sagittal plane and mid-sagittal surface optimization in brain MRI using a local symmetry measure. In: International Symposium on Medical Imaging 2005, San Diego, CA, Proceedings of SPIE, SPIE; 2005]. p. 568–79.

Talairach J, Tournoux P. Co-planar stereotaxic atlas of the human brain: 3-dimensional proportional system: an approach to cerebral imaging, vol. 39 of Thieme classics. New York: G. Thieme; 1988].

Thomann PA, Wustenberg T, Pantel J, Essig M, Schroder J. Structural changes of the corpus callosum in mild cognitive impairment and Alzheimer's disease. Dement Geriatr Cogn Disord 2006];21:215–20.

Toga AW, Thompson PM. Mapping brain asymmetry. Nat Rev Neurosci 2003];4:37–48.

Tzourio-Mazoyer N, Landeau B, Papathanassiou D, Crivello F, Etard O, Delcroix N, et al. Automated anatomical labeling of activations in spm using a macroscopic anatomical parcellation of the MNI MRI single-subject brain. Neuroimage 2002];15:273–89.

Verard L, Allain P, Travere JM, Baron JC, Bloyet D. Fully automatic identification of ac and pc landmarks on brain MRI using scene analysis. IEEE Trans Med Imaging 1997];16:610–6.

Volkau I, Bhanuprakash K, Ananthasubramaniam A, Aziz A, Nowinski W. Extraction of the midsagittal plane from morphological neuroimages using the kullback-leibler's measure. Med Image Anal 2006];10:863–74.

Zhao L, Ruotsalainen U, Hirvonen J, Hietala J, Tohka J. Automatic cerebral and cerebellar hemisphere segmentation in 3D MRI: adaptive disconnection algorithm. Med Image Anal 2010];14:360–72.